Fundamental loading-curve characteristics of the persistent phosphor SrAl2O4:Eu2+,Dy3+,B3+: the effect of temperature and excitation density

Teresa Delgado, Nando Gartmann, Bernhard Walfort, Fabio Lamattina, Markus Pollnau, Arnulf Rosspeintner, Jafar Afshani, Jacob Olchowka, Hans Hagemann

ADVANCED PHOTONICS RESEARCH
Open Access
www.adpr-journal.com

Fundamental Loading-Curve Characteristics of the Persistent Phosphor $SrAl_2O_4:Eu^{2+},Dy^{3+},B^{3+}$: The Effect of Temperature and Excitation Density

Teresa Delgado, Nando Gartmann, Bernhard Walfort, Fabio LaMattina, Markus Pollnau, Arnulf Rosspeintner, Jafar Afshani, Jacob Olchowka, and Hans Hagemann**

The compound $SrAl_2O_4:Eu^{2+},Dy^{3+}$ is currently one of the best-performing persistent phosphors and numerous studies have been performed to understand the mechanisms involved in its afterglow process. One aspect which so far has received only limited attention is the dependence of loading curve characteristics on dopant concentrations. Herein, a detailed study of the loading curves of $SrAl_2O_4:Eu^{2+},Dy^{3+}$ as a function of composition, sample temperature, and pump intensity is presented, completed by emission decay and quantum yield measurements. The observed emission decays can be described using the Inokuti–Hirayama equation for a Dexter energy transfer (ET) process. As the Dexter ET rate and the electron transfer rate have a similar radial dependence, the Inokuti–Hirayama equation can also describe the electron transfer process involved for the trapping process. These observations indicate that in this persistent phosphor, the trapping process is a local process; however, different types of traps appear to present different "Dexter" critical radii R_0. This electron transfer is also temperature dependent, which requires further investigations.

1. Introduction

A persistent phosphor is a compound that keeps emitting light for seconds to hours after cutting the irradiation source. Its afterglow time is typically orders of magnitude longer than the luminescence lifetime of the excited state in which the emission originates. In inorganic persistent phosphors, two types of activation centers are located in the energy gap between the valence and the conduction band of the massif material: the emitters (rare earth or transition metal ions) and the traps (likewise rare earth or transition metal ions that act as codopants but also intrinsic lattice defects, impurities, etc). Hence, the persistent luminescence is governed by the slow liberation of trapped charge carriers at room temperature by a simple thermal de-excitation process. In addition, they can be charged and released over periods. This is the case of lanthanide-doped ceramics, and, among others, strontium aluminate $SrAl_2O_4$ doped with Eu^{2+} and Dy^{3+} shows one of the longest afterglows ever observed, lasting for several hours when codoped with B^{3+}.[1–3] The afterglow effect is explained by the existence of traps that are rapidly filled by electron transfer from the excited Eu^{2+} ions, and their energy is then slowly released via back transfer to the Eu^{2+} ions and subsequent luminescence.[3,4] Because of this feature, this product is in high demand for numerous applications,[5] such as security signs, jewellery, especially luminous watches, lighting of the cities,[6] highway engineering,[7,8]

T. Delgado, A. Rosspeintner, J. Afshani, H. Hagemann
Départment de Chimie Physique
Université de Genève
30, quai E. Ansermet, CH 1211 Geneva 4, Switzerland
E-mail: teresadelgado@chimieparistech.psl.eu;
hans-rudolf.hagemann@unige.ch

N. Gartmann, B. Walfort
LumiNova AG
Switzerland
Speicherstrasse 60a, CH-9053 Teufen, Switzerland

The ORCID identification number(s) for the author(s) of this article can be found under https://doi.org/10.1002/adpr.202100179.

DOI: 10.1002/adpr.202100179

F. LaMattina
Transport at Nanoscale Interfaces Laboratory
Swiss Federal Laboratories for Materials Science and Technology
Empa, Dübendorf CH-8600, Switzerland

M. Pollnau
Advanced Technology Institute
Department of Electrical and Electronic Engineering
University of Surrey
Guildford GU2 7XH, UK

J. Olchowka
CNRS
Univ. Bordeaux
Bordeaux INP
ICMCB UMR 5026
F-33600 Pessac, France

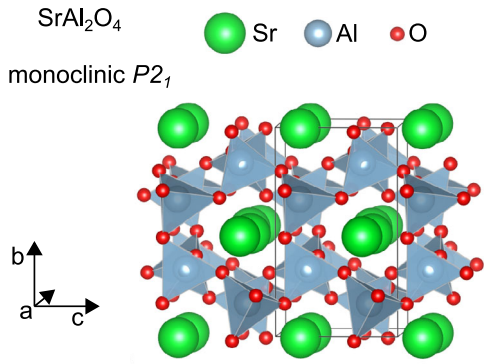

Figure 1. Room-temperature crystal structure of $SrAl_2O_4$ showing the coordination of Sr (in green) and the AlO_4 tetrahedral network.

noctilucent fibers,[6] or even fingerprint detection.[9] The well-known structure of $SrAl_2O_4$[10] is based on rings formed by six-corner-sharing aluminum oxide tetrahedra-forming channels. The Sr^{2+} ions are located within these channels on two different crystallographic sites, as shown in **Figure 1**.[10] Thus, when they are replaced by Eu^{2+} ions, two different emissions are observed in the blue and the green spectral region at around 450 and 520 nm, respectively.[11] Upon irradiation on the blue-emitting site, there is an energy transfer (ET) process to the green site that depends on the concentration of Eu^{2+}. Under 375 nm excitation, the nonexponential decay observed at 440 nm at 77 K can be quantitatively associated with the Förster ET process with $R_0 = 1.58(8)$ nm.[12] Further, blue emission is thermally quenched at room temperature.[13,14] When the latter compound is codoped with Dy^{3+}, the afterglow can increase to several hours.[15–17]

2. Background

Several studies have reported that the luminescence intensity of $SrAl_2O_4$:Eu^{2+},Dy^{3+} samples that were previously either kept in the dark for a long time or heated in the dark before the experiment to release all the thermal traps increases upon irradiation in the blue or near-UV region over a timespan of about 5−10 min before reaching a steady state.[4,18–20] These curves are called "loading curves" and are related to the trap-filling processes of the persistent phosphor. A first model of these loading curves was proposed by Jia using a simplified three-level system (Eu^{2+} ground state, Eu^{2+} excited state, and the trap state).[18] The solution of the model rate equations qualitatively reproduces the observed loading curves. However, fitting the experimental data required a superposition of three sets of curves. More recently, Smet and co-workers included an optically stimulated luminescence (OSL) process, which affects the loading of the traps.[19] Various experiments have revealed that there is a great variety of traps which are observed in $SrAl_2O_4$:Eu^{2+},Dy^{3+},B^{3+}.[14] Recently, Van der Heggen et al.[20] reported the presence of very deep traps with thermoluminescence (TL) peaks above 250 °C that have a very high trapping probability. The traps in $SrAl_2O_4$ can be intrinsic (i.e., defects in the crystal), as well as induced by the presence of B^{3+} or Dy^{3+}.[13,14,19–25]

The excitation spectra observed at 430 and 520 nm (Figure S1, Supporting Information) show that the emission at 430 nm is not excited above 410 nm, while the excitation band for the green emission extends up to 450 nm. It is thus possible to excite selectively the green-emitting Eu ion above 410 nm, while excitations at shorter wavelengths correspond to absorptions of both types of Eu ions in $SrAl_2O_4$. The blue emission is quenched at room temperature.[13] Thus, nonradiative decay also takes place. Further, as studied in detail by Bierwagen et al.,[13] ET takes place from the blue-emitting to the green-emitting Eu ions. Different TL curves have been observed for samples with different doping. **Figure 2** compares the normalized TL curves for samples S1($SrAl_2O_4$:1.5 mol%Eu^{2+}), S2($SrAl_2O_4$:1.5 mol%Eu^{2+},0.9wt%B), and S3($SrAl_2O_4$:1.5 mol%Eu^{2+},5 mol%Dy^{3+}), (Table 3 and 4 show all samples studied) excited at 445 nm (data from the study Bierwagen et al.[14]) to highlight the differences generated by the addition of boron and Dy, and Figure S2, Supporting Information, reveals the increase in TL intensity and shape induced by the progressive introduction of Dy^{3+}. These data correspond to the three different types of traps which are related to the green-emitting Eu ions. Exciting also the blue-emitting Eu ion (e.g., at 375 nm) leads to different TL curves[14] and shows that there is an additional set of traps which are reached only through the blue-emitting Eu ion. It is important to note that the afterglow corresponds exclusively to green emission at 520 nm.

This work is part of a series of systematic studies on $SrAl_2O_4$:Eu^{2+},Dy^{3+},B^{3+} to probe various contributions to the afterglow process as a function of relative dopant (Eu^{2+},Dy^{3+},B^{3+}) concentration, temperature, illumination wavelength, and intensity.[14,21] The introduction of boron which acts as a flux[22] adds additional traps and prevents Eu^{2+}oxidation.[23] The fundamental understanding of the trapping and detrapping processes is challenging, as these processes take place on extremely different time scales. The typical emission lifetime of Europium(2+) is in the microsecond range, and ET processes are typically much faster. On the other side, the loading and afterglow curves extend over minutes and hours, respectively. To grasp pertinent contributions to different processes, we present here an ensemble of loading curves as a function of sample composition, temperature, and irradiation intensity, together with luminescence decay and quantum yield experiments. The list of the different samples

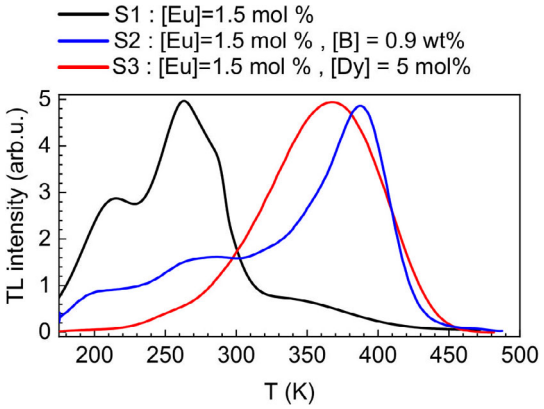

Figure 2. Smoothened TL curves measured for S1−S3 after loading at 173 K with 445 nm irradiation.

prepared and studied is given in the Experimental Section. These results show that a critical parameter is the ratio of available traps to excited Eu^{2+} ions, which affects loading curves, lifetimes, and quantum yield in a systematic way.

3. Results

3.1. Loading–Deloading Curves as a Function of Dopants, Sample Temperature, and Pump Intensity

Here we report the influence of the sample temperature (T_{exc}) and pump intensity (I_{exc}) on the loading experiments. The green emission at 525 nm was measured as a function of time upon continuous irradiation with a 447 nm light emission diode (LED) for 10 min. Experiments were carried out at various temperatures between $T_{exc} = 193$ and 298 K, and pump intensities range between $I_{exc} = 1.910$ and 0.191 μW/mm^2 (**Figure 3** and **4**). With the exception of S1 (1.5%Eu), for all other samples at low T_{exc}, the luminescence intensity during the loading process decreases with time, whereas at high T_{exc}, it increases with time. Botterman et al.[4] equally observed slightly decreasing loading curves at low temperature and increasing loading curves above ≈240 K.

In Figure 3, clear differences can be observed in the profile shape and in the dependence on pump intensity. For S1 (1.5%Eu), at high pump intensities the luminescence intensities decrease over time regardless of T_{exc} (Figure 3a). S2 (1.5%Eu, 0.9 wt%B) and S3 (1.5%Eu, 5%Dy) show a different behavior. At high I_{exc}, a monotonic increase over time is observed at $T_{exc} = 298$ K (Figure 4, red curves). When I_{exc} is lowered by half, down to 0.993 μW mm^{-2}, the measured intensities scale down accordingly. In addition, the general behavior in the three samples becomes similar (Figure 3 and 4). By investigating

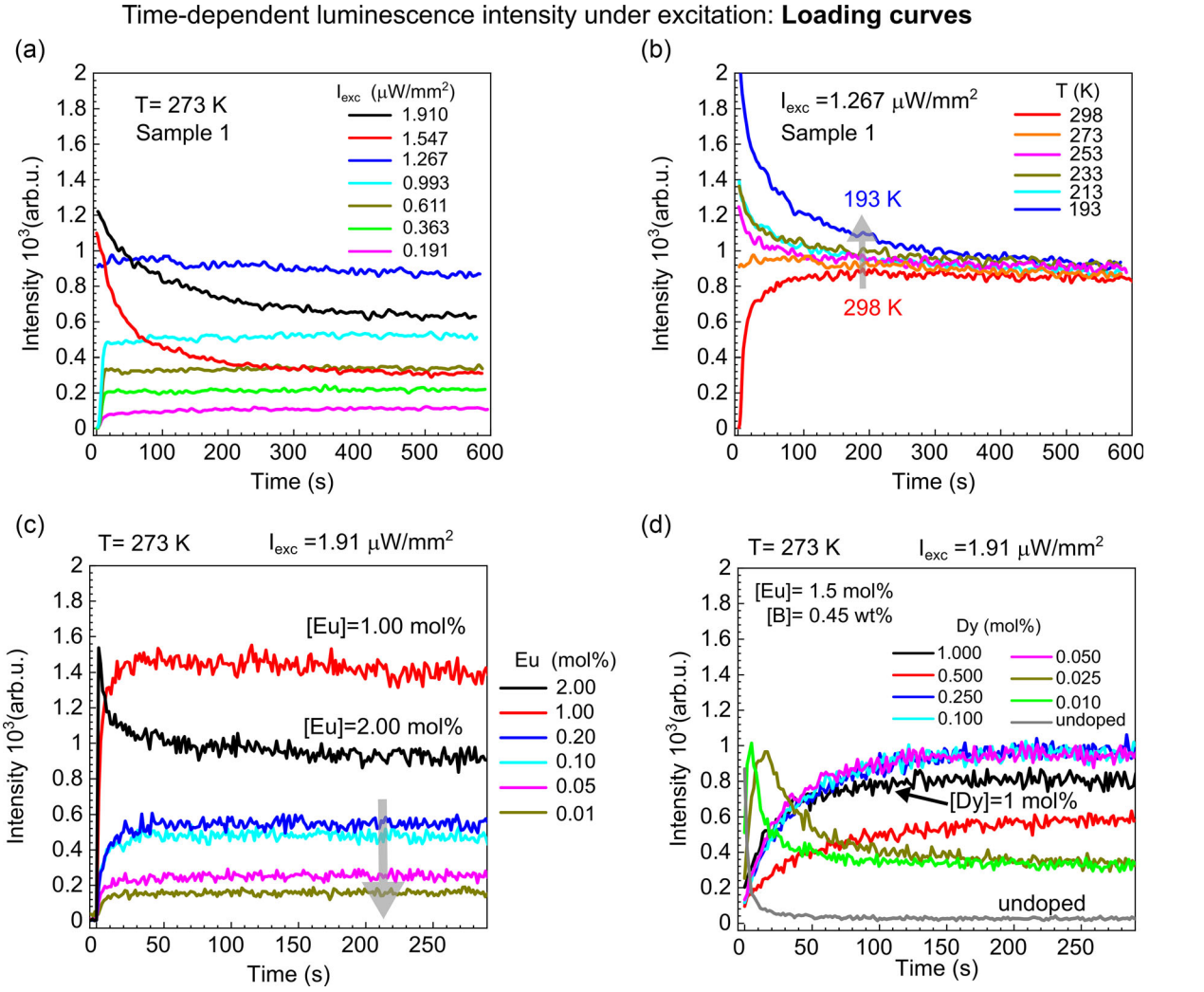

Figure 3. Time-dependent luminescence intensity at 520 nm under continuous-wave irradiation at 447 nm (loading curves). Before each loading cycle, the sample is heated up to 523 K for a total time of 2 min in the dark (see Figure S3a, Supporting Information). Loading curves for sample S1 ($SrAl_2O_4$:1.5 mol%Eu^{2+}): a) for different pump intensities at 273 K and b) for different temperatures for a fixed pump intensity of $I_{exc} = 1.267$ mW mm^{-2}. c) Loading curves for different Eu concentrations (samples S4–S9) at 273 K and $I_{exc} = 1.91$ μW mm^{-2}. d) Loading curves for different nominal Dy^{3+} concentrations (samples S10–S17) at 273 K and $I_{exc} = 1.91$ μW mm^{-2}.

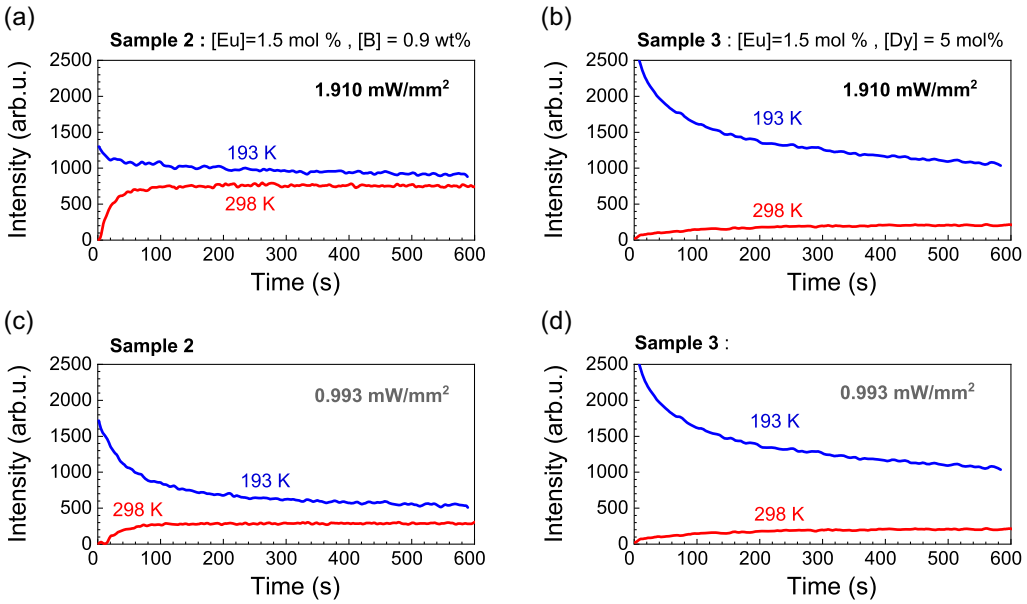

Figure 4. Loading curves of samples S2(1.5%Eu, 0.9wt%B) and S3 (1.5%Eu, 5%Dy) at different excitation temperatures and excitation densities.

the loading curves measured at intermediate values of T_{exc} and I_{exc}, such as in Figure 3a,b and Figure S4, Supporting Information, we can establish the critical range of temperature (T_{lim}) above which the curves switch their monotonic behavior over time from a decreasing to an increasing intensity profile with time. We observe that all the changes of trend are located at 273 K, except for S1 (1.5%Eu) at the lowest I_{exc} for which T_{lim} decreases to 233 K and at the highest I_{exc} for which T_{lim} increases and the profile does not switch (**Table 1**). In the presence of B and Dy, however, at maximum I_{exc}, the switch is observed at 273 K (Table 1 and Figure S4, Supporting Information). In fact, increasing concentrations of Eu^{2+} (Figure 3c) and Dy^{3+} (Figure 3d) within the host leads to the switch at room temperature.

In contrast, for S1 (1.5%Eu) and S2 (1.5%Eu, 0.9 wt%B) at constant I_{exc}, the steady state is reached after ≈10 min of irradiation and presents the same-steady state intensities at $T_{exc} = 193$ and 298 K (see as an example sample S1 at $I_{exc} = 1.267\ mW\ mm^{-2}$ and variable T_{exc} in Figure 3b). S3 (1.5%Eu, 5%Dy), however (see Figure 4), reaches a higher steady-state intensity at low temperature than at high temperature.

3.2. Room-Temperature Luminescence Decay Measurements as a Function of Dopants and Pump Intensity

The green luminescence decay curves of the samples have been measured at room temperature under excitation at 355 nm and detection above 500 nm, at different I_{exc}. It must be noted that under excitation at 355 nm, both blue- and green-emitting Eu^{2+} ions are excited, but equivalently to the loading−deloading experiments, only the green luminescence has been detected (see Figure S3c, Supporting Information). The corresponding decay curves at the highest I_{exc} (2.55 μW mm^{-2}, see Experimental Section) are presented in **Figure 5** and **6**.

As previously observed by the decay curves of Eu^{2+}-[13] or Eu^{2+},Dy^{3+}-doped $SrAl_2O_4$[19] at room temperature, the biexponential equation

$$I(t) = A_1 e^{-\frac{t}{\tau_1}} + A_2 e^{-\frac{t}{\tau_2}} \quad (1)$$

can be used to fit satisfactorily these decay curves.

It is interesting to note that biexponential fits were recently reported also for Eu-doped $Sr_4Al_{14}O_{25}$.[24] The authors obtained lifetimes of ≈448−301 and 45−68 ns for Eu1 and ≈729−934 ns and 146−237 ns for Eu2 (see Table S2, Supporting Information).

Recent time-resolved experiments[12] show that at 77 K, the emission at 520 nm shows under 437 nm excitation a single monoexponential decay with the same lifetime of 1120 ns for five Eu-,Dy-codoped samples (Eu 0.75%, 1%, and 1.5% with Dy 0.25% and Eu 0.01% with Dy 0.1% and 0.5%). Figure S5, Supporting Information, illustrates the monoexponential decay observed at 5 K for sample S1. This experiment shows that there is only one emitting species present, which is apparently in contrast with the observation of a double-exponential decay, which

Table 1. T_{lim} (K) for different samples and I_{exc} (μW/mm^2).

I_{exc} / Sample	0.191	0.363	0.611	0.993	1.267	1.547	1.910
S1 (1.5%Eu)	233	273	273	273	273	Decreasing profile at all *T*.	Decreasing profile at all *T*.
S2 (1.5%Eu, 0.9 wt%B)	–	–	273	273	–	–	273
S3 (1.5%Eu, 5%Dy)	273	273	273	273	273	273	273

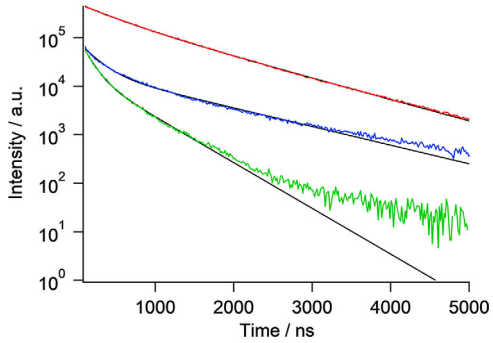

Figure 5. Biexponential fit of the decay curves for sample S1 (1.5%Eu) in red, sample S2 (1.5%Eu, 0.9wt%B) in blue, and sample S3 (1.5%Eu, 5% Dy) in green.

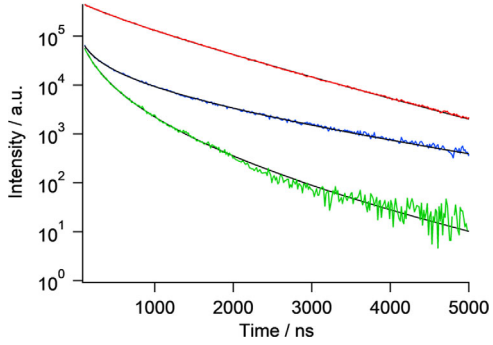

Figure 6. Inokuti–Hirayama fit of the decay curves for sample S1 (1.5% Eu) in red, sample S2 (1.5%Eu, 0.9wt%B) in blue, and sample S3 (1.5%Eu, 5%Dy) in green.

from classical kinetics implies that there are two emitting species.

Alternatively, the decay curves can also be fit using the Inokuti–Hirayama equation involving a Dexter expression for the electron transfer process.[25] Indeed, Equation 23 from the study by Inokuti et al.[25] is

$$\phi(t) = \exp\left(-\frac{t}{\tau_0} - \gamma^{-3} \times \frac{c}{c_0} \times g\left(e^{\gamma} \times \frac{t}{\tau_0}\right)\right) \tag{2}$$

where $\gamma = \frac{2R_0}{L}$ and $g(z) = -z\int_0^1 \exp(-zy) \cdot (\ln y)^3 \mathrm{d}y$. R_0 is the "critical transfer distance," L a constant called the "effective average Bohr radius," c the acceptor (trap) concentration, and c_0 the critical transfer concentration: $c_0 = \frac{3}{4\pi R_0^3}$.

According to the IUPAC Gold Book, the Dexter energy exchange rate is given by[26]

$$k_{\mathrm{ET}} \propto \frac{h}{2\pi} \times P^2 \times J \times e^{-\frac{2r}{L}} \tag{3}$$

r is the donor–acceptor distance, L and P constants, and J the spectral overlap integral. For electron exchange, the radial dependence of the rate constant is given by Equation (2) and (5) in the classical paper by Brunschwig et al.[27–29]

$$k(r) \propto H_{\mathrm{AB}}^2 = (H_{\mathrm{AB}}^0)^2 \times e^{-\beta \cdot (r-\sigma)} \tag{4}$$

where H_{AB} is the electronic coupling element and σ the hard sphere radius. If one equates the parameter β with $2/L$, the radial dependence of the rate constant for ET and electron transfer becomes identical, and thus the Inokuti–Hirayama equation for the Dexter ET can also be used to describe electron transfer.

Figure 5 and 6 compare the experimental data with the fitting functions (biexponential and Inokuti–Hirayama) and the corresponding residuals are given in Figure S6, Supporting Information.

Figure 5 shows that the biexponential fit agrees very well with the experimental data below 1500 ns, while the Inokuti–Hirayama fit (Figure 6) shows excellent agreement with the data over the entire range of data points measured (5000 ns). We have also tried to fit the data using the Inokuti–Hirayama[30] static quenching model via Förster resonance ET.

$$\phi(t) \propto \exp\left(-\frac{t}{\tau} - \frac{4\pi^{3/2}}{3} c R_0^3 \sqrt{\frac{t}{\tau}}\right) \tag{5}$$

which resulted in poorer fits.

The fitted parameters using the Inokuti–Hirayama Equation (2) are given in **Table 2**.

For sample S1, the fitted value of τ_0 is in the range of the lifetime of 1120 ns measured at 77 K,[12] which is expected, as the thermal quenching of the emission at 520 nm is observed at higher temperatures; the emission quenching temperature at which the emission intensity is half of the low-temperature intensity is around 400 K.[13] However, the fitted value of τ_0 is much larger for samples S2 and S3. The TL of samples S2 and S3 under 375 nm excitation showed strong TL peaks starting at 200–220 K,[14] and it is thus possible that at room temperature, these low-temperature TL peaks result at room temperature in an afterglow in the microsecond range, leading to a larger value of τ_0. For sample S1, the ratio c/c_0 is the smallest, and it becomes about 10 times larger for samples S2 and S3. It must be noted however that for these samples, the value of γ (and consequently the value of R_0) increases strongly. It appears that the electron transfer described with the Dexter model is quite different in sample S1 compared with samples S2 and S3.

Additional decay measurements were performed on samples S1, S2, and S3 with the attenuated power of laser excitation, using metal mesh filters (see Experimental Section). For sample S1, the normalized decay curves are identical within the experimental error (see Figure S7, Supporting Information). However, this is not the case for samples S2 and S3 (Figure S8 and S9, Supporting Information). The results are presented in Table S3, Supporting Information. In both cases, the initial decay becomes faster with decreasing laser power (down to 3%).

Table 2. Fitting parameters of the decay curves using Equation (2).

Sample	τ_0 [ns]	c/c_0	γ
S1	1255	0.27	2.9
S2	2348	3.91	14.0
S3	2840	4.46	6.27

The Inokuti–Hirayama fits show some scatter of the parameters (see Table S2, Supporting Information). For samples S2 and S3, the faster initial decay at low powers can be associated with an increase of the value of c/c_0 and an increase of the value of γ (and thus also of R_0) with decreasing laser power. This behavior can qualitatively be associated with competition for the electron trapping process. At low power, more traps are available, while at high power, parts of the traps have been already filled by other excited Eu^{2+} ions. In the case of sample S1, the number of accessible traps is very low compared with samples S2 and S3, so with the same laser power, the high power limit of the electron transfer process is reached.

3.3. Room-Temperature Quantum Yield Measurements as a Function of Composition and Excitation Wavelength

The intrinsic quantum yield (Q_{int}) was measured for all three reference samples at different excitation wavelengths **(Figure 7)**. The highest value of Q_{int} is observed for S1 (1.5%Eu) under blue excitation at 440 nm, that is, when exciting solely the green-emitting Eu^{2+} ions. Agreement of the Q_{int} values with the corresponding lifetimes can be verified by estimating Q_{int} through the lifetimes at room temperature and at 3 K. For instance, in Figure S5, Supporting Information, the green emission decay of sample S1 is shown at 3 K. A monoexponential decay with a lifetime of $\tau_2 = 1184$ ns is obtained. Fitting the decay data for sample S1 at room temperature approximately using a monoexponential, one obtains a value of ≈867 ns, which leads to an estimate of Q_{int} of 0.72. This Q_{int} value obtained through the lifetimes is in very good agreement with the one obtained in the integrating sphere of pure green emission after excitation at 440 nm, $Q_{int} = 0.68$. For samples 2 and 3, the estimated values of $Q_{int} = 0.51$ and $Q_{int} = 0.22$, respectively, from the lifetimes agree reasonably well with the values of $Q_{int} = 0.63$ and $Q_{int} = 0.17$ obtained in the integrating sphere of pure green emission after excitation at 440 nm. For all three samples, the value of Q_{int} is lower for excitation at 375 nm compared with excitation at 440 nm. This observation is in agreement with the results obtained by Smet et al.[19] This reduction in quantum yield can be explained by the fact that at 375 nm, both blue- and green-emitting ions are excited (see Figure S1, Supporting Information) and that blue emission is quenched at room temperature and has a higher chance of being in their ground state. At 77 K, the ratio of the extinction coefficients at 375 nm of the blue-emitting Eu ion versus the green-emitting ion was found to be 0.6 ± 0.2,[12] that is, about 40% of the light is absorbed by the blue-emitting Eu ion at that wavelength. The thermal quenching of the blue emission removes thus the fraction of photons absorbed by the blue-emitting ions. Quantum yield experiments have previously been performed on Eu-only doped single crystals with Eu concentrations of 0.5%, 1.0%, 2.0%, 2.5%, and 3.0%.[30] Under 374 nm excitation, the quantum yield was reported to be 35%, 35%, 49%, 50%, and 45%, respectively. The quantum yield value for sample S1 with 1.5% Eu^{2+} of ≈42% is in between the values for samples with 1% and 2% Eu^{2+} obtained by Nakauchi et al.[30] The increase of quantum yield with concentration can be explained by the increased ET which competes with the thermal quenching of the blue-emitting Eu^{2+} ions.

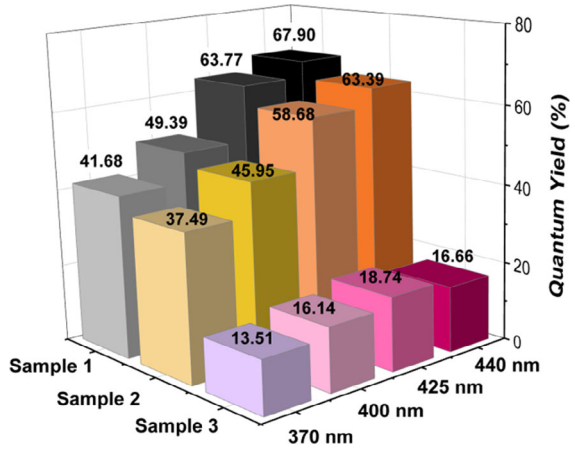

Figure 7. Results of room-temperature Q measurements of samples S1 (1.5%Eu), S2 (1.5%Eu, 0.9wt%B), and S3 (1.5%Eu, 5%Dy) at different excitation wavelengths.

The presence of boron in sample S2 leads to a small reduction of the Q_{int} values for all wavelengths (see Figure 7). The addition of Dy^{3+} (S3) leads to a dramatic reduction in quantum yield. These sample-dependent reductions of Q_{int} correlate with the changes of the emission lifetimes reported earlier.

4. Discussion

Various experiments have revealed that there are a great variety of traps which are observed in $SrAl_2O_4$:Eu^{2+},Dy^{3+},B^{3+}.[14] Recently, Van der Heggen et al.[20] reported the presence of very deep traps with TL peaks above 250 °C that have a very high trapping probability. The traps in $SrAl_2O_4$ can be intrinsic (i.e., defects in the crystal), as well as induced by the presence of B^{3+} or Dy^{3+}. Different TL curves have been observed for samples with different doping. Figure 2 compares the normalized TL curves for samples 1– to illustrate the different types of traps generated by the different dopings[14] and Figure S2, Supporting Information, reveals the increase in TL intensity and shape induced by the progressive introduction of Dy^{3+}. As seen in Figure S2, Supporting Information, the overall TL intensity increases significantly with increasing Dy content, confirming that the presence of Dy generates many more accessible traps for the afterglow. This is also seen by the comparison of the intensity of the afterglow curves of differently doped samples.[14] With 447 nm excitation, only the green-emitting Eu^{2+} ion is excited. This excitation can lead to the green emission observed at 520 nm or to filling of the different types of traps either directly (thermally assisted[11] and/or tunneling) or via the conduction band.[31] The applicability of the Inokuti–Hirayama equation based on a Dexter process indicates that the trapping process is rather a local process.

The depletion of traps can take place either by thermal excitation or by OSL.[19] It is important to note also that the TL intensity increases with the excitation temperature, that is, that at T_{exc} = room temperature, and many more traps become accessible than at $T_{exc} = -100$ °C (see Figure S10, Supporting Information, with data from the study by Bierwagen et al.[13]).

Our results presented earlier show that the relative number of accessible traps increases from S1(1.5%Eu) to S3(1.5%Eu,5%Dy).

Previous temperature-dependent TL results[4,14] showed for S3 that there are many accessible relatively shallow traps at room temperature compared with the traps created by codoping with B (TL peak at 400 K in Figure 2). With samples S4−S9, we explore the ratio of intrinsic traps with respect to the total number of Eu^{2+} ions. The isovalent substitution of Sr^{2+} by Eu^{2+} is not expected to lead to additional defects in the $SrAl_2O_4$ samples, as one can obtain solid solutions from $SrAl_2O_4$ to $EuAl_2O_4$.[32] This fact also supports the assumption that the nominal Eu^{2+} concentration is close to the real concentration.[33] Thus, the amount of intrinsic traps can be assumed to remain constant with the same synthesis protocol; however, the amount of Eu^{2+} is tuned. With samples S10−S17, the number of Dy^{3+}-related traps is increased systematically (see Figure S2, Supporting Information).

Introducing boron and, in particular, Dy^{3+} ions leads to significantly faster decay in the first 1000 ns (Figure 5 and 6). This behavior is also reflected by the quantum yield experiments shown in Figure 7. As for 440 nm excitation, the quantum yield decreases from 68% for sample S1 to 17% for sample S3. This huge loss in quantum efficiency confirms that the trapping rate is much faster than the radiative rate. However, as has been shown by Van der Heggen et al.,[34] only an estimated fraction of 1.6% of the Eu^{2+} ions participates in the trapping process, which generates an afterglow. One other aspect which comes into play is the possible nonradiative decay channel of the trap, which so far has not been addressed as well. The photoconductivity experiments by Ueda et al[31] clearly show the onset of photoconductivity upon excitation at 430 nm at temperatures of 200 K and above, while below 200 K, shorter wavelengths (400 nm and below) were required to observe photoconductivity. The combination of these results suggests that the electron transfer to the traps may be followed also by the release of electrons into the conduction band, in addition to the back relaxation to the emitting Eu^{2+} ion.

In Figure 3c, we have compared the loading curves for different Eu^{2+} concentrations. If one assumes that the number of intrinsic defects is independent of Eu^{2+} concentration for these samples, as the isovalent substitution of Sr^{2+} by Eu^{2+} is not expected to generate additional defects (note also that both ions have very similar ionic radii; thus, no local distortion from chemical pressure is expected[35]), then the ratio of the number of traps with respect to the total number of Eu^{2+} ions decreases with increasing Eu^{2+} doping. We observe that at low Eu^{2+} concentrations, the trapping dominates and increasing loading curves are observed, while at high Eu^{2+} concentration, the behavior is inversed (see Figure 3c). This observation also correlates with the unusual behavior observed for the quantum yield as a function of the Eu^{2+} concentration shown in Figure S11, Supporting Information: at very low Eu^{2+} concentration, the quantum yield is low, as the trapping proportion is important. With increasing concentration, the relative trapping process is decreased and the quantum yield increases up to a maximum value until it starts to decrease by concentration quenching processes.

It appears thus that the critical parameter is the ratio of available traps to excitable Eu^{2+} ions. If this ratio is high (such as in Dy-doped samples or samples with very low Eu^{2+} doping), then increasing loading curves are observed. This is illustrated by the behavior observed with increasing Dy doping: Figure 3d shows the loading curves obtained with increasing nominal Dy^{3+} doping and concomitantly the evolution from a decreasing loading curve to an increasing loading curve. Further, the very dilute Eu^{2+}-doped samples have a much lower quantum yield than the samples with 1% doping, and also the Dy^{3+}-codoped samples have very low quantum yields compared with the Eu^{2+}-doped samples, as shown in Figure 7. Thus, the trend of the loading curves correlates also with the observed quantum yields, which are associated with the ratio of traps to excitable Eu^{2+} ions.

Another parameter which comes into play is the pump rate. A decreasing loading curve behavior is observed experimentally for the highest pump intensities in Figure 3a. At lower pump intensities (between 1.2 and 0.2 $\mu W\,mm^{-2}$), the trend switches from slightly decreasing to slightly increasing. This observation can be explained with the fact that with higher pump power, more Eu^{2+} ions are excited, but the total number of traps remains the same; thus, with high power, the ratio of traps/excited Eu^{2+} ions is low, resulting in a decreasing loading curve.

Finally, we can address the influence of temperature. We see that with increasing temperature, there is a transition from a decreasing to an increasing loading curve around 273 K, as shown in Figure 3b. We have shown earlier[14,21] that with increasing excitation temperature, additional traps become thermally accessible (see Figure S10, Supporting Information), and these additional traps contribute to a significant increase of the TL curves below ≈60 °C. These data show that the ratio of the number of accessible traps with respect to the number of excited Eu^{2+} ions is also strongly affected by temperature.

Tydtgat et al.[36] proposed a model for the trapping and detrapping process in persistent phosphors, which takes into account the temperature and the irradiation intensity. This model considers an activation energy for both the trapping and thermal quenching processes, which was found to be about 0.4 eV for $Sr_2MgSi_2O_7$:Eu,Dy for both processes, as well as an OSL process. This model is indeed a good starting point for further developments. We have shown in this article that loading curves, decay curves, and quantum yield depend on the trap concentration, which implies that trap concentration must be explicitly included. The activation energy involved for electron transfer (extracted from temperature-dependent decay curves using the Inokuti−Hirayama model) should correspond to the activation energy for trapping appearing in the loading curves. This remains to be established. Further, to account for the significant drop in quantum yield for Dy^{3+},B^{3+}-codoped samples, it may become necessary to include also a loss for trap depletion (injection of charges in the conduction band).

5. Conclusion

The data presented here show that the trapping process in the persistent phosphor $SrAl_2O_4$:Eu^{2+},B^{3+},Dy^{3+} can be strongly modulated by the concentration of the dopants, temperature, illumination wavelength, and power. The analysis of the decay curves suggests that the loading process is a local electron transfer, as the Dexter ET rate constant (included in the Inokuti−Hirayama equation) and the electron transfer rate constant present similar radial dependence. The qualitative result is that a significant fraction of the excited Eu^{2+} ions can reach eventually the traps within the "Dexter" radius R_0 and contribute to the initial faster decays observed. Note that the "Dexter" radius is not the same, depending

on the doping. For the corresponding loading curves, once all the traps are filled, a steady-state emission results.

For a more complete description, one must consider also the second (blue-emitting) Eu^{2+} ion, which can be excited with irradiation below 400 nm. As it was shown previously,[12,13] ET takes place between the Eu ions on different Sr sites. As the blue emission is quenched at room temperature, there is a loss of photons which is reflected both in a lower quantum efficiency below 400 nm (see Figure 7) and in the lower integrated afterglow intensity for irradiation at 382 nm compared with irradiation at 444 nm with the same pump intensity.[12]

The critical parameter is the ratio of the number of accessible traps with respect to the number of excited Eu^{2+} ions. This ratio is a function of dopants, irradiation wavelength, and power, as well as of temperature. We have shown here that this ratio influences the shape of the loading curves, the emission decay curves, and also the quantum yield. All these parameters must be considered if one wants to establish a quantitative model which describes simultaneously in a unified way all the experimental properties. Finally, the loading temperature dependence is not unique to strontium aluminate phosphors,[37] which suggests that a temperature-dependent loading process needs to be fundamentally understood for persistent phosphors.

6. Experimental Section

Synthesis: Doped $SrAl_2O_4$ samples were synthesized by a solid-state reaction. Sample S1 contained only Eu^{2+}, sample S2 contained Eu^{2+} and B^{3+}, and sample S3 Eu^{2+} and Dy^{3+} (see **Table 3**). Stoichiometric amounts of $SrCO_3$ (purity >99%) and Al_2O_3 (purity >99.99%) together with Eu_2O_3 (1.5 mol%, purity >99.9%) for sample S1, 0.9 wt% of boric acid (purity >99.9%) for sample S2, and Dy_2O_3 (5.0 mol%, purity >99.9%) for sample S3 were thoroughly mixed using a ball mill. The ratio Al/(Sr + Eu) was fixed exactly to 2/1. The mixtures were then annealed for 4 h under reducing conditions at 1450 °C (5% H_2 in argon) in a tube furnace. X-ray diffraction (XRD) measurements confirmed that in all samples more than 93% of the main compound was in the $SrAl_2O_4$[13] phase. Additional samples with systematic Eu^{2+} or Dy^{3+} concentration variations were also prepared (see **Table 4**). The powders were then pressed into 10 mm-diameter pellets made from a mixture of 300 mg of KBr and 100 mg of sample material, which were ground together before pressing to ensure compactness and homogenous distribution of the sample.

Loading Experiments: The same homemade TL setup previously described[21] was used for the present experiment with some modifications. During the trap loading process, the green emission at 520 nm was recorded for 10 min under continuous irradiation with a 447 nm LED and with a 500 nm long-pass (LP) edge filter in front of the detector (see Figure S3b-c, Supporting Information). This process was performed at different excitation temperatures (193, 213, 233, 253, 273, and 298 K) and at different pump intensities (1.910, 1.547, 1.267, 0.993, 0.611, 0.363, and 0.191 μW mm^{-2}) by use of different gray filters to reduce the excitation light intensity (none, 81%, 66%, 52%, 32%, 19%, 10%, respectively) situated after the 447 nm LED. Before each loading cycle, the sample was heated up to 523 K for a total time of 2 min in the dark for thermal release of the traps. The temperature profile and scheme of experimental conditions are given in Figure S3a, Supporting Information. For calculating the pump intensity, the total pump power irradiated into the sample (150 μW) was divided by the surface of the aforementioned pellet (78.54 mm^2), that is, 1.91 μW mm^{-2} or 0.191 mW cm^{-2} without a gray filter.

Lifetime Measurements: For measuring the luminescent lifetime of Eu^{2+} in $SrAl_2O_4$:Eu^{2+} at room temperature, the same pellets described earlier were used. The samples were excited at 355 nm with a Q-switched frequency-tripled Nd:YAG laser (pulse duration: ≈5 ns), operating at a repetition rate of 20 Hz (Quantel). A 500 nm LP edge filter was placed in front of the detector to reproduce the same conditions as in the loading–deloading experiment. The emitted light was collected with a telescope and refocused into a fiber bundle to direct the light to a monochromator (Shamrock), equipped with a gated charge coupled device (CCD) camera (Andor). Metal mesh optical filters with transmittances of 50, 43, 30.2, 22, 17, 6, and 3% were used to reduce the incident pump intensity, which was 2.55 μW mm^{-2} or 0.255 mW cm^{-2}, down to 1.275, 1.097, 0.770, 0.561, 0.434, 0.153, and 0.077 μW mm^{-2}. It was important to note that this was the average pump intensity of 20 pulses of 5 ns duration (20 Hz repeat frequency), that is, the instantaneous power was very high. The luminescence decay was recorded during a total time of 6.5 μs.

Quantum Yield Measurements: The room-temperature quantum yield (Q) measurements were performed using a Quantum Phi Horiba integration sphere at four different excitation wavelengths (370, 400, 425, and 440 nm) and at a continuous wave (CW) pump intensity over the different wavelengths of 1.15 μW mm^{-2}, a value which was in the range of the pump intensities used for the loading–deloading experiments. In this case, the samples were not pressed in the form of pellets but the phosphor powder was dispersed in a rounded Teflon sample holder of 10 mm diameter, specially designed for Q measurements. That is, the same irradiated surface as for the pellets was considered (78.54 mm^2). For more information on the experimental details of Q measurements in this persistent phosphor, see our previous publications.[33] The reproducibility of Q measurements is proven in Table S1, Supporting Information.

Table 3. Composition of the main $SrAl_2O_4$ samples.

Sample	Eu [mol%]	B [wt%]	Dy [mol%]	Comment
S1	1.5	0	0	Usual Eu^{2+} concentration
S2	1.5	0.9	0	Effect of boron
S3	1.5	0	5	Effect of dysprosium

Table 4. Composition of the additional $SrAl_2O_4$ samples with systematic Eu^{2+} or Dy^{3+} concentration variations.

Sample	Eu [mol%]	B [wt%]	Dy [mol%]	Comment
S4	2.00	0	0	Changing Eu^{2+} concentration
S5	1.00	0	0	
S6	0.20	0	0	
S7	0.10	0	0	
S8	0.05	0	0	
S9	0.01	0	0	
S10	1.5	0.45	1.000	
S11	1.5	0.45	0.500	
S12	1.5	0.45	0.250	
S13	1.5	0.45	0.100	Changing Dy^{3+} concentration
S14	1.5	0.45	0.050	
S15	1.5	0.45	0.025	
S16	1.5	0.45	0.010	
S17	1.5	0.45	0	

Supporting Information

Supporting Information is available from the Wiley Online Library or from the author.

Acknowledgements

This work was supported by the Swiss National Science Foundation (projects 200020_182494 and 200021_169033 and Postdoc. Mobility P400P2_191108/1) and the KTI (project number 25902.1 PFNM-NM and 15217.1 PFIW-IW).

Conflict of Interest

The authors declare no conflict of interest.

Data Availability Statement

The data that support the findings of this study are available from the corresponding author upon reasonable request.

Keywords

charging curves, loading afterglow materials, persistent materials, strontium aluminates

Received: June 23, 2021
Revised: November 11, 2021
Published online:

[1] V. Vitola, D. Millers, I. Bite, K. Smits, A. Spustaka, *Mater. Sci. Technol.* **2019**, *35*, 1661.
[2] Y. Li, M. Gecevicius, J. Qiu, *Chem. Soc. Rev.* **2016**, *45*, 2090.
[3] R. E. Rojas-Hernandez, F. Rubio-Marcos, M. Á. Rodriguez, J. F. Fernandez, *Renew. Sustain. Energy Rev.* **2018**, *81*, 2759.
[4] J. Botterman, J. J. Joos, P. F. Smet, *Phys. Rev. B* **2014**, *90*, 085147.
[5] D. Poelman, D. Van der Heggen, J. Du, E. Cosaert, P. F. Smet, *J. Appl. Phys.* **2020**, *128*, 240903.
[6] S. Wu, Z. Pan, R. Chen, X. Liu, *In Long Afterglow Phosphorescent Mater.*, Springer International Publishing, New York **2017**.
[7] J. Botterman, P. F. Smet, *Opt. Express* **2015**, *23*, A868.
[8] I. Bite, G. Krieke, A. Zolotarjovs, K. Laganovska, V. Liepina, K. Smits, K. Auzins, L. Grigorjeva, D. Millers, L. Skuja, *Mater. Des.* **2018**, *160*, 794.
[9] L. Liu, Z. Zhang, L. Zhang, Y. Zhai, *Forensic Sci. Int.* **2009**, *183*, 45.
[10] A.-R. Schulze, H. K. M. Buschbaum, Z. Für Anorg. *Allg. Chem.* **1981**, *475*, 205.
[11] S. H. M. Poort, W. P. Blokpoel, G. Blasse, *Chem. Mater.* **1995**, *7*, 1547.
[12] B. Walfort, N. Gartmann, J. Afshani, A. RossPeintner, H. Hagemann, *J. Rare Earths*, https://doi.org/10.1016/j.jre.2021.07.014.
[13] J. Bierwagen, S. Yoon, N. Gartmann, B. Walfort, H. Hagemann, *Opt. Mater. Express* **2016**, *6*, 793.
[14] J. Bierwagen, T. Delgado, G. Jiranek, S. Yoon, N. Gartmann, B. Walfort, M. Pollnau, H. Hagemann, *J. Lumin.* **2020**, 117113.
[15] T. Matsuzawa, Y. Aoki, N. Takeuchi, Y. Murayama, *J. Electrochem. Soc.* **1996**, *143*, 2670.
[16] P. Dorenbos, *J. Electrochem. Soc.* **2005**, *152*, H107.
[17] F. Clabau, X. Rocquefelte, S. Jobic, P. Deniard, M. H. Whangbo, A. Garcia, T. Le Mercier, *Chem. Mater.* **2005**, *17*, 3904.
[18] D. Jia, *Opt. Mater.* **2003**, *22*, 65.
[19] D. Van der Heggen, J. J. Joos, P. F. Smet, *ACS Photonics* **2018**, *5*, 4529.
[20] D. Van der Heggen, D. Vandenberghe, N. K. Moayed, J. De Grave, P. F. Smet, J. J. Joos, *J. Lumin.* **2020**, *226*, 117496.
[21] H. Hagemann, D. Lovy, S. Yoon, S. Pokrant, N. Gartmann, B. Walfort, J. Bierwagen, *J. Lumin.* **2016**, *170*, 299.
[22] T.-P. Tang, C.-M. Lee, F.-C. Yen, *Ceram. Int.* **2006**, *32*, 665.
[23] S. Yoon, J. Bierwagen, M. Trottmann, B. Walfort, N. Gartmann, A. Weidenkaff, H. Hagemann, S. Pokrant, *J. Lumin.* **2015**, *167*, 126.
[24] H. Liu, X. Liu, X. Wang, M. Peng, P. Xiong, Y. Chen, Y. Wang, B. Lei, Q. Zeng, *J. Am. Ceram. Soc.* **2020**, *103*, 5758.
[25] M. Inokuti, F. Hirayama, *J. Chem. Phys.* **1965**, *43*, 1978.
[26] A. D. McNaught, A. Wilkinson, *IUPAC Gold Book. IUPAC. Compendium of Chemical Terminology*, Blackwell Scientific Publications, **1997** Oxford https://doi.org/10.1351/goldbook.D01654.
[27] B. S. Brunschwig, S. Ehrenson, N. Sutin, *J. Am. Chem. Soc.* **1984**, *106*, 6858.
[28] J. W. Verhoeven, *Pure Appl. Chem.* **1996**, *68*, 2223.
[29] E. J. Piechota, G. J. Meyer, *J. Chem. Educ.* **2019**, *96*, 2450.
[30] D. Nakauchi, G. Okada, M. Koshimizu, T. Yanagida, *J. Lumin.* **2016**, *176*, 342.
[31] J. Ueda, T. Nakanishi, Y. Katayama, S. Tanabe, *Phys. Status Solidi C* **2012**, *9*, 2322.
[32] F. Meister, M. Batentschuk, S. Dröscher, A. Osvet, A. Stiegelschmitt, M. Weidner, A. Winnacker, *Proc. 6th Eur. Conf. Lumin. Detect. Transform. Ioniz. Radiat. LUMDETR 2006* **2007**, *42*, 771.
[33] T. Delgado, J. Afshani, H. Hagemann, *J. Phys. Chem. C* **2019**, *123*, 8607.
[34] D. Van der Heggen, J. J. Joos, D. C. Rodríguez Burbano, J. A. Capobianco, P. F. Smet, *Materials* **2017**, *10*, 867.
[35] V. D'Anna, L. M. L. Daku, H. Hagemann, F. Kubel, *Phys. Rev. B* **2010**, *82*, 024108.
[36] C. Tydtgat, K. W. Meert, D. Poelman, P. F. Smet, *Opt. Mat. Express* **2016**, *6*, 844.
[37] J. Du, O. Q. De Clercq, D. Poelman, *Sci. Rep.* **2019**, *9*, 10517.